International Journal of Rock Mechanics & Mining Sciences 48 (2011) 67–76

Contents lists available at ScienceDirect

International Journal of Rock Mechanics & Mining Sciences

journal homepage: www.elsevier.com/locate/ijrmms

A finite element implementation of strain-softening rock mass

Shuilin Wang*, Hong Zheng, Chunguang Li, Xiurun Ge

State Key Laboratory of Geomechanics and Geotechnical Engineering, Institute of Rock and Soil Mechanics, Chinese Academy of Sciences, Wuhan 430071, PR China

ARTICLE INFO

Article history:
Received 4 January 2010
Received in revised form
15 June 2010
Accepted 15 November 2010

Keywords:
Strain-softening
Finite element analysis
Brittle-plasticity
Rock mass

ABSTRACT

Many types of rock masses behave in a strain-softening way in geotechnical engineering. Numerical methods have to be used to study these kinds of media. But a limit to the rate of softening of the strain-softening material exists within the framework of the classical theory of plasticity. Considering the salient characteristic that the strength parameters decrease during the process of strain-softening, this paper develops a procedure for modeling strain-softening behavior based on the methodology for analyzing brittle-plastic rock mass. In the proposed procedure, strain-softening process is simplified as a series of stress drops and plastic flow. Therefore, solving a strain-softening problem becomes finding a series of brittle-plastic solutions. The proposed procedure is implemented in a finite element code based on the classical theory of plasticity in which Mohr–Coulomb (M–C) criterion is employed. Numerical examples are examined and the results validate the proposed implementation.

1. Introduction

Experimental research of mechanical properties of rock mass shows that there are four types of post-failure curves from the uniaxial or triaxial compression test of rock specimens [1]. The classification of stress–strain curves constitutes the basis of establishing four corresponding constitutive models phenomenologically. They are elasto-perfectly brittle-plastic, elasto-plastic strain-softening, elasto-perfectly plastic and elasto-plastic strain-hardening models. The elasto-perfectly plastic model indicates that the strength parameters keep constant after the material strength reaches its peak value. Strain-hardening model indicates that the strength parameters increase in plastic state as the deformation accrues. Elasto-perfectly plastic and strain-hardening behavior only appears when confining pressure is high in rock test. Strain-softening model displays that the strength parameters decrease gradually from peak values to residual ones with increasing deformation in post-failure region, and the strain-softening behavior is often observed both in laboratory and in the field of underground rock engineering [2,3]. Elastic-brittle-plastic model implies that the strength parameters drop abruptly from peak values to residual ones in post-failure region, and perfectly brittle-plastic phenomenon can be considered to be a special case of strain-softening behavior.

Elastic-brittle-plastic and strain-softening phenomena are usually accompanied by strain localization in which irreversible deformation is located in narrow zones of limited thickness. In geomaterials such as rock and soil, fractures or shear bands will appear in the narrow zones where the strength parameters decrease. Perfectly brittle-plastic and strain-softening phenomena have been studied from both micro-mechanical and macroscopic viewpoints. The micro-mechanical approach analyses the interaction between the granular particles [4,5] or the crystal grains of the material [6]. The onset and extension of the microcracks in the material are described and strain-softening behaviors of specimens in laboratory tests are reproduced [7–10]. A complete review on micromechanics was given by Kemeny and Cook [10].

Considering the strength parameter weakening in the processes of strain-softening, the macroscopic approach models the overall behavior of the strain-softening material on the basis of the results of large scale (with respect to the size of the soil/rock particles) tests and of field observations, without going into the details of the interaction between its microscopic components.

If attention is paid to the process of the strain localization in macroscopic methods, different techniques for modeling of localized deformation are available, including the use of the Cosserat continuum [11,12], the non-local theory [13,14], gradient-dependent formulations [15–17], strong discontinuity approaches [18,19], weak discontinuity approaches [20–21] and other approaches that the effect of the band is smeared over the crossing element [22–24]. Most of the above techniques are based on non-conventional definitions of the continuum and they are used to overcome difficulties related to inception and development of localization or to mesh dependence when numerical analyses are performed. Bardet [25], Pietruszczak and Xu [26] and Sterpi [27] presented comprehensive reviews, respectively, while they studied localization and strain-softening behavior of materials such as soil, concrete and similar cemented mixtures.

On the other hand, if concern is focussed on the failure zone's distribution and the degree of deformation in practice, some simpler approaches based on the classical continuum theory, such as Lo and Lee [28], Sterpi [27], Zhang and Subhash [29], Hajiabdolmajida et al. [30],

* Corresponding author Tel.: +86 27 87199227; fax: +86 27 87199560.
E-mail address: slwang@whrsm.ac.cn (S. Wang).

1365-1609/$ - see front matter © 2010 Elsevier Ltd. All rights reserved.
doi:10.1016/j.ijrmms.2010.11.001

Zheng et al. [1], as well as continuous damage models [31–35], are also practical. Although these macroscopic approaches present some drawbacks in catching the onset and extension of the narrow zone of the strain localization and explaining the mechanism of the formation of the localization with respect to the micro-mechanical approach, and there might exist mesh dependency to a certain extent in using numerical approaches, estimation of the plastic zone and the degree of failure are quite accurate [1,36]. From practical engineering perspectives, the extent of the plastic zone and the degree of failure are quite useful for the design of reinforcement in the construction of slopes and underground caverns. Therefore, the macroscopic approaches based on the classical continuum theory have still been adopted in geotechnical engineering and the obtained results are welcome for engineers.

In this paper, a new procedure for modeling the strain-softening process is developed and a finite element implementation is presented under the framework of the classical theory of plasticity. Numerical results validate the proposed methodology. The paper is organized in the following way. In Section 2, the types of post-failure behaviors in rock mechanics tests are discussed and the implementation of the corresponding constitutive model in numerical methods is briefly reviewed. Section 3 presents the simplification of the stress–strain curve in the softening stage based on the brittle–plastic model and modeling of strain-softening relation. The main steps of the implementation of solving the strain-softening problems in finite element method (FEM) are presented in Section 4. Numerical examples are examined and the results show the effectiveness of the proposed methods, and analysis of the excavation of an underground cavern is also carried out in Section 5. Conclusions are given in Section 6.

2. Types of stress–strain curves of rock mass and their modeling

2.1. Types of stress–strain curves of rock mass and consideration on numerical modeling

Fig. 1(a) schematically gives a set of stress–strain curves observed in laboratory test of rock and soil specimen. For simplicity, they are typically classified as four types, i.e. perfectly brittle-plastic (curve I), strain-softening (curve II), perfectly plastic (curve III) and strain-hardening (curve IV) relationship as shown in Fig. 1(b).

The modes of treating the perfectly plastic and strain-hardening relationship in numerical methods are mature within the framework of classical theory of plasticity and they can be easily implemented in FEM, etc. For perfectly brittle-plastic and strain-softening constitutive model, Lo and Lee [28] were the pioneers who described the abrupt decrement of strength from the peak to the residue, implemented the model in finite element code and performed the stability analysis of a slope. While studying brittle rock mass, Zheng et al. [1] proposed a detailed procedure for calculating the abrupt change in stresses from the peak strength surface to the residual strength surface and presented the analytical method for brittle-plastic model and numerical implementation in FEM. In the analysis, the stresses are dropped from the peak strength surface to the residual strength surface and then plastic flow will continue in the post peak regime.

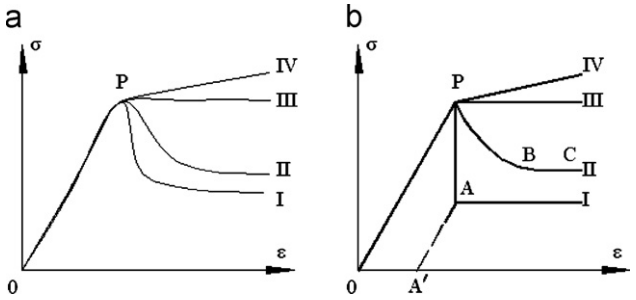

Fig. 1. (a) Stress–strain curves observed in laboratory test of rock and soil specimen, (b) idealized stress–strain curve for different models.

In the same way as deriving the stress–strain relationship of strain-hardening material, the stress–strain relationship in strain-softening model can be obtained by subdividing the plastic modulus into the plastic modulus of the perfectly plastic behavior and the softening modulus. It seems that the strain-softening constitutive relationship can be implemented in numerical methods like strain-hardening model. However, ill-posed problems may arise in the post peak regime, and the stress–strain relationship becomes meaningless when the rate of softening is high [1]. Therefore, care must be taken in dealing with strain-softening constitutive model.

2.2. Incremental stress–strain relationship under the classical theory of plasticity

For elasto-plastic media, suppose that the yield function is

$$F(\sigma,\kappa)=0 \tag{1}$$

where σ represents the stress tensor, and κ is a growth (hardening, softening, etc) function that defines the size of the yield surface. The parameter κ also represents the plastic loading history of the material, and can be written as $\kappa=\kappa(\eta)$, in which η is a parameter indicating the change of strength parameters. For example, η is the softening parameter when strain-softening behavior is considered.

If the loading condition

$$\left(\frac{\partial F}{\partial \sigma}\right)^T D d\varepsilon > 0 \tag{2}$$

is satisfied, the stress–strain relationship in an infinitesimal increments is given by [37]

$$d\sigma = D_{ep} d\varepsilon \tag{3}$$

at a given stress state and plastic deformation history, where

$$D_{ep} = D - D_p, D_p = \frac{1}{M} D \frac{\partial Q}{\partial \sigma} \left(\frac{\partial F}{\partial \sigma}\right)^T D \tag{4}$$

D_{ep}, D and D_p are the matrices in plasticity constitutive theory, $d\varepsilon$ represents incremental strain components, and $Q(\sigma)$ is the potential function. The real number M is defined as

$$M = A + \left(\frac{\partial F}{\partial \sigma}\right)^T D \left(\frac{\partial Q}{\partial \sigma}\right) \tag{5}$$

and the real number A is

$$A = -\frac{\partial F}{\partial \kappa} \frac{d\kappa}{d\lambda} \tag{6}$$

For hardening materials, the real number $A>0$, for perfectly plastic materials $A=0$, and for strain-softening materials $A<0$.

In numerical analysis, the external forces are applied in load steps with finite sizes. The resulting displacements and stresses with incremental form have finite size, too. Then Eq. (3) is replaced by

$$\Delta\sigma = \int_0^{\Delta\varepsilon} D_{ep} d\varepsilon \tag{7}$$

The incremental constitutive relationship has to be integrated numerically to compute incremental stress ($\Delta\sigma$) from incremental strain ($\Delta\varepsilon$). This means that D_{ep} should be an integrable matrix function at a given stress state.

2.3. Limitation of classical theory of plasticity for softening material

In an elasto-perfectly plastic or elasto-plastic strain-hardening material, it is well known that D_{ep} is always integrable and that numerical integration in Eq. (7) can be carried out without question. But in the case of softening, $A<0$. In order for the constitutive matrix (D_{ep}) to be meaningful, the following condition must be met:

$$|A| < \left(\frac{\partial F}{\partial \sigma}\right)^T D \frac{\partial Q}{\partial \sigma}, \quad A<0 \tag{8}$$

In fact, if $|A|=(\partial F/\partial\sigma)^T D(\partial Q/\partial\sigma)$, then $M=0$. This makes D_{ep} indeterminant. If $|A|>(\partial F/\partial\sigma)^T D(\partial Q/\partial\sigma)$ and $A<0$, then $M<0$. Hence, D_{ep} can be written as $D_{ep}=D+|M|^{-1}d_Q d_F^T$ with $d_Q=D(\partial Q/\partial\sigma)$ and $d_F=D(\partial F/\partial\sigma)$. Then Eq. (3) can be written as

$$d\sigma = \left(D+\frac{1}{|M|}d_Q d_F^T\right)d\varepsilon \tag{9}$$

Pre-multiplying Eq. (9) with $d\varepsilon^T(\neq 0)$ leads to

$$d\varepsilon^T d\sigma = d\varepsilon^T D d\varepsilon + \frac{1}{|M|}d\varepsilon^T d_Q d_F^T d\varepsilon. \tag{10}$$

If the associated flow rule is used, $Q=F$, and then $d_Q=d_F$. The above equation can be further written as

$$d\varepsilon^T d\sigma = d\varepsilon^T D d\varepsilon + \frac{1}{|M|}(d\varepsilon^T d_F)^2 \tag{10.1}$$

The elasticity matrix D is positive definite, hence $d\varepsilon^T D d\varepsilon>0$. Furthermore, $|M|^{-1}(d\varepsilon^T d_F)^2$ is not negative. This leads to $d\varepsilon^T d\sigma>0$. However, $d\varepsilon^T d\sigma<0$ in the process of strain-softening. Eq. (10.1) contradicts the definition of strain-softening for the associated flow rule. If non-associated flow rule is used, $d_Q\neq d_F$. Eq. (10) can then be written as

$$d\varepsilon^T d\sigma = d\varepsilon^T D d\varepsilon + \frac{1}{|M|}\left(\left(\frac{\partial Q}{\partial\sigma}\right)^T d\sigma^e\right)\left(\left(\frac{\partial F}{\partial\sigma}\right)^T d\sigma^e\right) \tag{10.2}$$

where $d\sigma^e=Dd\varepsilon$. Assume that the potential function is in the similar form as failure function and that it is convex. Both $(\partial Q/\partial\sigma)^T d\sigma^e>0$ and $(\partial F/\partial\sigma)^T d\sigma^e>0$ in loading condition. This also leads to $d\varepsilon^T d\sigma>0$, which is inconsistent with the definition of strain-softening. Therefore, for softening material, a constitutive relationship can be determined only if its softening rate satisfies inequality (8). In other words, there will be a limit of softening rate when D_{ep} is computed by Eqs. (4)–(6).

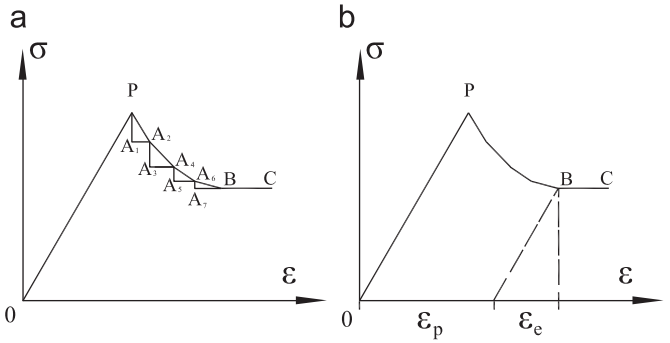

Fig. 2. (a) Illustration of simplification of strain-softening process, (b) elastic and plastic strains in the strain-softening curve.

3. Simplification of strain-softening process and modeling of strain-softening relation

Since numerical solution process will be in trouble when a rock with high strain-softening rate is dealt within the same way as in elasto-plastic strain-hardening model, a new approach must be developed in order to remove the aforementioned drawbacks during the constitutive integration. After studying the principle of analyzing brittle-plastic rock mass and considering the similar features that the stress decreases as the plastic strain increases for brittle-plastic and strain-softening material, we think that the methodology of solving brittle-plastic problem is heuristic.

3.1. Simplification of strain-softening process

In Fig. 2(a), the idealized stress–strain curve for strain-softening rock consists of part 'OP', 'PB' and 'BC'. The relationship of stress and strain in part 'OP' is considered as linear. Part 'PB' is in the process of strain-softening and part 'BC' is in the residual stage. During the strain-softening stage, strength parameters decrease as the softening parameter, which can be defined as a function of plastic strain, increases, and they reach their residual values when the softening parameter is greater than a limit. Fig. 2(b) shows that the limit of the softening parameter can be determined from the plastic strains corresponding to point 'B' in the strain-softening curve.

For the stress–strain curve of strain-softening rock, the relationship of stress and strain in strain-softening stage is normally nonlinear. The piecewise linear approximation is made when numerical analysis is performed under the framework of the classical theory of plasticity. Fig. 2(a) shows that curve 'PB' is replaced by piecewise linear segments 'PA_2', 'A_2A_4', 'A_4A_6' and 'A_6B' and each segment usually has different negative slope. Here, the piecewise linear segments are further simplified and they are treated in a stepwise manner.

For example, the strain-softening segment 'PA_2' is simplified to be stress drop part 'PA_1' and plastic flow part 'A_1A_2'. Strain-softening process from 'P' to 'A_2' becomes brittle-plastic one from 'P' to 'A_1' and then from 'A_1' to 'A_2'. The simplification can be made for the other segments in the same way. Thereby, the strain-softening process can be regarded as a series of brittle-plastic steps as shown in Fig. 2(a). Solving directly the strain-softening problem comes down to finding a series of brittle-plastic solutions.

3.2. Incremental stress–strain relationship for brittle-plastic model

After the strain-softening process is simplified to be a series of brittle-plastic steps, the key element of solving the strain-softening problem is to find the solution to brittle-plastic problem. According to the approach proposed in [1] under the framework of classical plastic theory, the stresses reach a certain point 'P' on the peak strength surface(PSS) by loading from a certain initial state and will fall on a point 'A' on the residual strength surface (RSS) with a sudden change if the loading condition is satisfied, and then stresses will change on RSS, as shown in Fig. 3. Therefore, the incremental stresses consist of two parts after the stresses reach PSS.

In each step, denote PSS by $F_p(\sigma,\kappa)=0$ and RSS by $F_r(\sigma,\kappa)=0$, where σ represents stress tensor and κ is a parameter indicating the change of strength parameters.

During the brittle-plastic process, the stress increments can be written as

$$\Delta\sigma = \Delta\sigma^d + \Delta\sigma^f \tag{11}$$

where $\Delta\sigma$ is the total stress increment, $\Delta\sigma^d$ the stress increment by stress drop and $\Delta\sigma^f$ the stress increment caused by stress flow

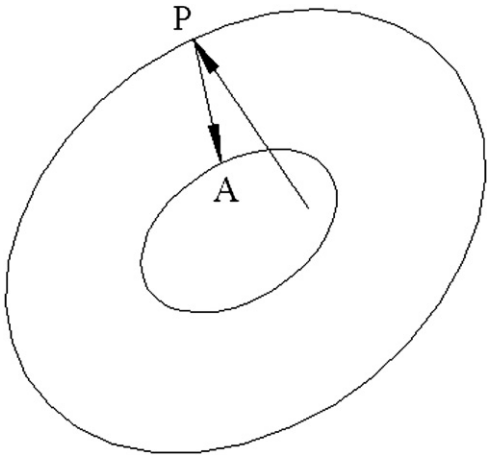

Fig. 3. Diagram of stress drop in stress space.

on RSS. The term $\Delta\sigma^f$ can be computed from Eq. (3) and it is written as

$$\Delta\sigma^f = D_{ep}\Delta\varepsilon \tag{12}$$

The stress drop ($\Delta\sigma^d$) is determined by the stress change from PSS to RSS, and the computation of it will be discussed in detail in the next subsection. The incremental stress–strain relationship with the form of finite sizes is

$$\Delta\sigma = \Delta\sigma^d + \int_0^{\Delta\varepsilon} D_{ep}\,d\varepsilon \tag{13}$$

3.3. Computation of stress drop

In the last subsections, it is illustrated that the strain-softening process is replaced by a series of brittle-plastic steps, and the stress increment in each brittle-plastic step is divided into stress increment by stress drop and the stress increment by plastic flow.

As to the computation of stress drop in numerical procedure, three hypotheses on stress-dropping are discussed in [1]. Based on our numerical experiences, different hypotheses will influence the computation time and the accuracy. The convergent results will be trivially altered because the stresses in the media will be adjusted to meet the equilibrium during the iteration.

Here, the assumption of the constant minor principal stress is made and M–C criterion is employed to illustrate how the incremental stresses caused by stress drop are computed.

Denote Cartesian stress tensors by σ_{ij} and the three principal stresses by $\sigma_i (i=1,3)$. Suppose that $\sigma_{ip} (i=1,3)$ is on PSS and $\sigma_{ir} (i=1,3)$ on RSS and that the directions of the principal stresses are unchanged after the stress drop. The variations of the magnitude of the three principal stresses are

$$\Delta\sigma_i = \sigma_{ir} - \sigma_{ip} (i=1,3) \tag{14}$$

If the M–C yield criterion is used, it is written in principal stress space as

$$F(\sigma_1,\sigma_3,\eta) = \sigma_1 - \alpha\sigma_3 - Y = 0 \tag{15}$$

in which $\alpha = (1+\sin\varphi)/(1-\sin\varphi)$, $Y = 2c\cos\varphi/(1-\sin\varphi)$, c and φ are cohesion and the internal friction angle, respectively, σ_1 is the major principal stress, and σ_3 the minor principal stress.

When stresses reach the peak strength,

$$F_p(\sigma_{1p}, \sigma_{3p},\eta) = \sigma_{1p} - \alpha_p\,\sigma_{3p} - Y_p = 0 \tag{15a}$$

In Eq. (15a), $\alpha_p = (1+\sin\varphi_p)/(1-\sin\varphi_p)$, $Y_p = 2c_p\cos\varphi_p/(1-\sin\varphi_p)$.

After the stresses drop to the RSS,

$$F_r(\sigma_{1r}, \sigma_{3r},\eta) = \sigma_{1r} - \alpha_r\sigma_{3r} - Y_r = 0 \tag{15b}$$

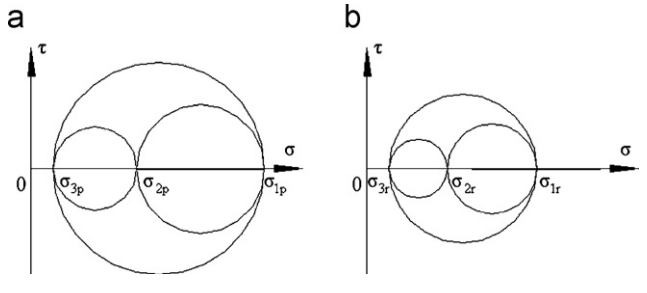

Fig. 4. Mohr's diagram, (a) principle stress components on PSS; (b) principle stress components on RSS.

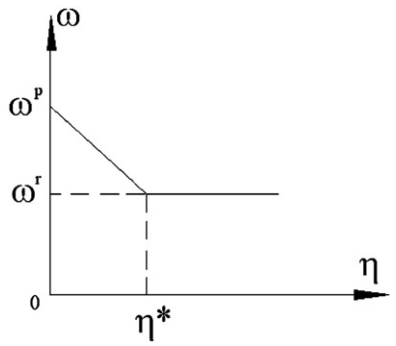

Fig. 5. Evolution of strength parameters.

where α_r and Y_r have the same meaning as those in Eq. (15a). Subscripts '*p*' and '*r*' indicate that the parameters are in their peak and residual values in Eqs. (15a) and (15b), respectively.

As a constant minor principal stress is assumed, we have

$$\Delta\sigma_3 = \sigma_{3r} - \sigma_{3p} = 0 \tag{16}$$

Substracting Eq. (15a) from Eq. (15b), the difference of the major principal stress before and after the stress drop is

$$\Delta\sigma_1 = \sigma_{1r} - \sigma_{1p} = (\alpha_r - \alpha_p)\sigma_{3r} + Y_r - Y_p \tag{17}$$

Fig. 4 indicates the state of stress at a point which is represented by the Mohr diagram. Assume that the ratio of the difference of the principal stresses is constant before and after the stress drop, i.e. $(\sigma_{2r}-\sigma_{3r})/(\sigma_{1r}-\sigma_{3r}) = (\sigma_{2p}-\sigma_{3p})/(\sigma_{1p}-\sigma_{3p})$, then.

$$\Delta\sigma_2 = \sigma_{2r} - \sigma_{2p} = \sigma_{3r} + \frac{\sigma_{2p}-\sigma_{3p}}{\sigma_{1p}-\sigma_{3p}}(\sigma_{1r}-\sigma_{3r}) - \sigma_{2p} \tag{18}$$

From Eqs. (16)–(18), the principal stress increments caused by stress drop can be calculated after the strength parameters corresponding to the peak and residual ones are determined. The incremental principal stresses are transformed back into the Cartesian coordinate system under the assumption that the directions of the three principal stresses are unchanged during the stress drop, and the incremental stress vector ($\Delta\sigma^d$) in Eq. (13) is then obtained.

3.4. Evolution of strength parameters

During the strain-softening stage, strength parameters decrease while the softening parameter increases. Here the softening parameter is defined as the plastic shear strain ($\eta = \varepsilon_1^p - \varepsilon_3^p$), which is the difference between the major and minor principal plastic strains.

For simplicity, the parameters are described by bilinear functions of plastic shear strain

$$\omega(\eta) = \begin{cases} \omega_p - (\omega_p - \omega_r)(\eta/\eta^*) & 0 < \eta < \eta^* \\ \omega_r & \eta \geq \eta^* \end{cases} \tag{19}$$

where ω represents any one of the strength parameters, such as c, φ and ψ, etc. η^* is the critical plastic shear strain from which the residual behavior starts and should be identified by experiments. Fig. 5 shows the rule of evolution of strength parameters. If η^* is small, the softening slope is steep, and the slope is gentle if η^* is large.

4. Numerical procedure in solving strain-softening problem

4.1. Algorithm for constitutive integration

The crux of the finite element implementation of the proposed method is constitutive integration, namely, how to calculate the stress increments from the given strain increments. The algorithm for constitutive integration is stated below.

For the rth iteration of each load increment, comply with the following steps:

(1) Compute $\Delta\sigma_e^r = D\Delta\varepsilon^r$ and the try stress $\sigma_e^r = \sigma^{r-1} + \Delta\sigma_e^r$, where the subscript e denotes that elastic behavior is assumed;
(2) Check if σ_e^r is beyond the PSS. If the answer is negative, the response is elastic and σ^r is set equal to σ_e^r. Or else brittle-plastic process is considered.

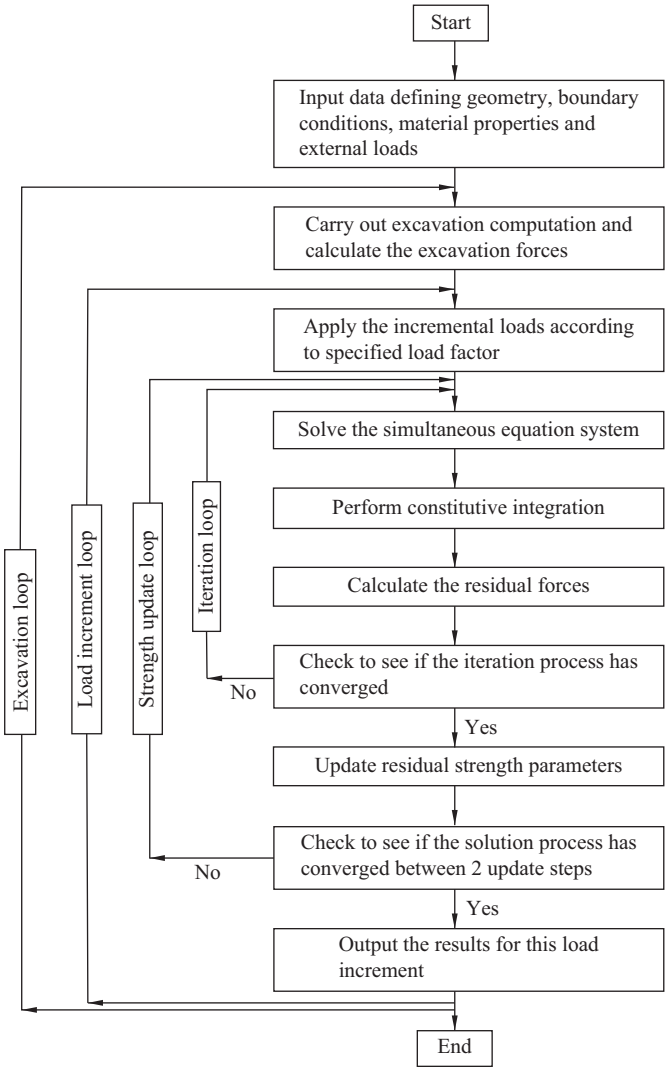

Fig. 6. Numerical flow chart for the proposed method.

(3) Compute $\Delta\sigma^d$, $\Delta\sigma^f = \int_0^{\Delta\varepsilon} D_{ep}d\varepsilon$ and $\Delta\sigma^r = \Delta\sigma^d + \Delta\sigma^f$. Firstly, compute the principal stress increment $\Delta\sigma_i\,(i=1,\ 3)$ from Eqs. (16)–(18) based on the peak and residual strength parameters at the current load step. Then, $\Delta\sigma^d$ is obtained by transformation. $\Delta\sigma^f$ is calculated on the condition that the stresses should meet Eq. (15b).
(4) Accumulate the stresses as $\sigma^r = \sigma^{r-1} + \Delta\sigma^r$.
(5) Check to see if the iteration process has converged. If yes, compute the plastic strains and the plastic shear strain ($\eta = \varepsilon_1^p - \varepsilon_3^p$), and update strength parameters by Eq. (19). Go to the next iteration if no.

In step 3, if the Gauss point has not previously yielded and it has yielded during the application of load corresponding to the current iteration (i.e. rth iteration), $\Delta\sigma^r = \beta D\Delta\varepsilon + \Delta\sigma^d + \int_0^{(1-\beta)\Delta\varepsilon} D_{ep}d\varepsilon$. The parameter β is determined by $F_p(\sigma^{r-1} + \beta D\Delta\varepsilon) = 0$.

In the above main steps, the PSS and RSS are generally different at each Gauss point in each load step. The peak strength parameters of each Gauss point are updated at the end of each load step. The residual strength parameters will be updated at the end of the iteration process in a new load step. The computation of $\Delta\sigma^d$ and $\Delta\sigma^f$ should be carried out carefully at each iteration.

4.2. Numerical procedure in solving strain-softening problem

Because the presented method is based on the framework of the classical theory of plasticity, the numerical procedures for the finite element implementation of strain-softening behavior are similar to those discussed in [37]. However, the procedures are complicated with the consideration of strain-softening model.

A general flow chart that summarizes the implementation of the proposed method is shown in Fig. 6. In the flow chart, the strength update loop is added when strain-softening model is dealt with by the proposed method. In each strength update step, iterations are carried out until convergence is achieved. Then the residual strength parameters are updated. And then a new strength update step begins. For geotechnical engineering, excavation is the routine work. The excavation loop is also included in the program.

5. Analysis of numerical examples

5.1. Example 1. A circular tunnel excavated in a strain-softening rock mass

A circular tunnel excavated in isotropic rock mass under hydrostatic stress field is considered firstly. Body force is ignored. Geometric and mechanical parameters are presented in Table 1 where two kinds of M–C rock mass with #1 and #2 are considered. During the softening stage, the cohesion c and friction angle φ are

Table 1
Geometric and mechanical parameters.

M–C rock mass	#1	#2
Radius of tunnel, r_0 (m)	3	3
Initial stress, σ_0 (MPa)	5	5
Young's modulus, E (GPa)	10	10
Poisson's ratio (v)	0.25	0.25
η^*	0.008	0.008
c_p (MPa)	1.0	1.0
c_r (MPa)	0.7	0.7
φ_p (deg)	30	30
φ_r (deg.)	22	22
ψ_p (deg.)	3.75	15.0
ψ_r (deg.)	3.75	0.0

decreased except the dilatancy angle ψ in rock mass #1, but c, φ and ψ all are decreased in rock mass #2.

Although there is no analytical symmetric solution available for this problem, approximate solutions can be obtained by some numerical methods developed by [38–40], according to which the plastic zone appears around the tunnel when internal pressure p_i is lower than $p_c=0.3268\sigma_0$. The excavation force around the tunnel surface is simulated in 'n'($=5$) load steps when the elastic-plastic transition is started. It means that the internal pressure p_i on the tunnel surface decreases from p_c to complete unloading in five steps with each load step $\Delta p=(p_c-0)/5$ during the excavation, whereas elastic deformation happens when p_i changes from the initial state with $p_i=\sigma_0$ to the state with $p_i=p_c$ and the elastic reaction can be easily dealt with and it is not described here.

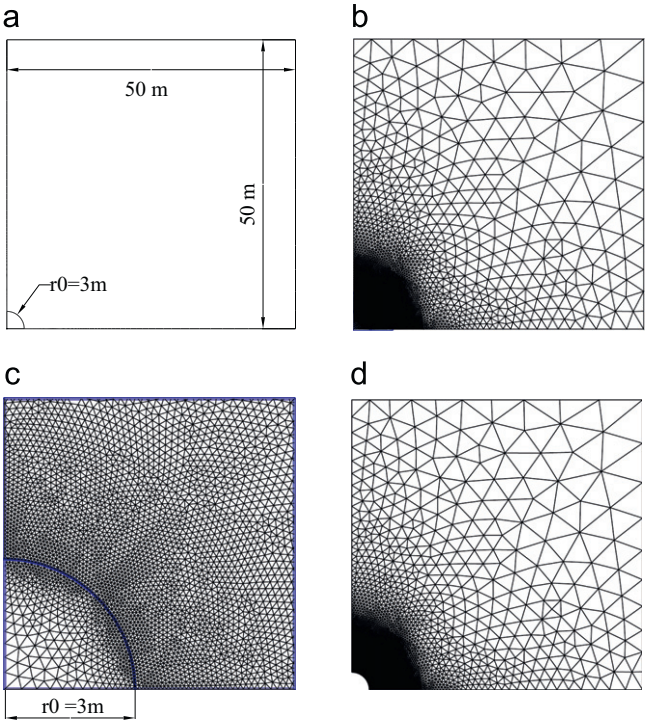

Fig. 7. (a) Geometry of the model, (b) finite element mesh,(c) finite element mesh around the tunnel, (d) finite element mesh after the excavation.

Varas et al. [36] studied the bifurcation in the problem of unloading a circular excavation in a strain-softening material by FLAC, and they revealed that the solutions are basically equivalent for the full meshes and the quarter meshes. Hereupon, only one quarter of the circular tunnel model is used for computer efficiency as far as the aims of this study are concerned. The model area is 50 m $\times$ 50 m (Fig. 7a) and it is sufficiently large to avoid undesirable boundary effects. Fig. 7(b) shows the finite element mesh with 11172 three-node elements and 5708 nodes, which corresponds to tunnel wall mesh sizes of $r_0/40$. A local area around the tunnel is displayed in Fig. 7(c) to show the fineness of the mesh, and Fig. 7(d) illustrates the mesh after the tunnel is excavated.

Three different meshes (see Fig. 8) corresponding to tunnel wall mesh sizes of $r_0/10$, $r_0/20$ and $r_0/40$ are considered to demonstrate the influence of the mesh fineness on the computation accuracy. By means of the proposed numerical procedure, ground response curves and evolution of plastic radii are obtained as shown in Fig. 9 for rock mass #1 and Fig. 10 for rock mass #2. The comparisons of the results by FEM and those by approximate methods indicate that different grids result in different numerical accuracy. The finer the mesh is, the higher the accuracy is. This is what is expected in FEM. Therefore, the mesh corresponding to tunnel wall mesh sizes of $r_0/40$ is employed in the following analysis.

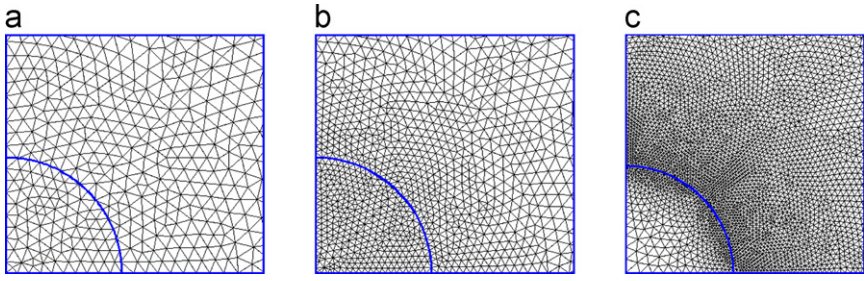

Fig. 8. Three different meshes employed, (a) mesh size in tunnel wall: $r_0/10$, (b) mesh size in tunnel wall: $r_0/20$,(c) mesh size in tunnel wall: $r_0/40$.

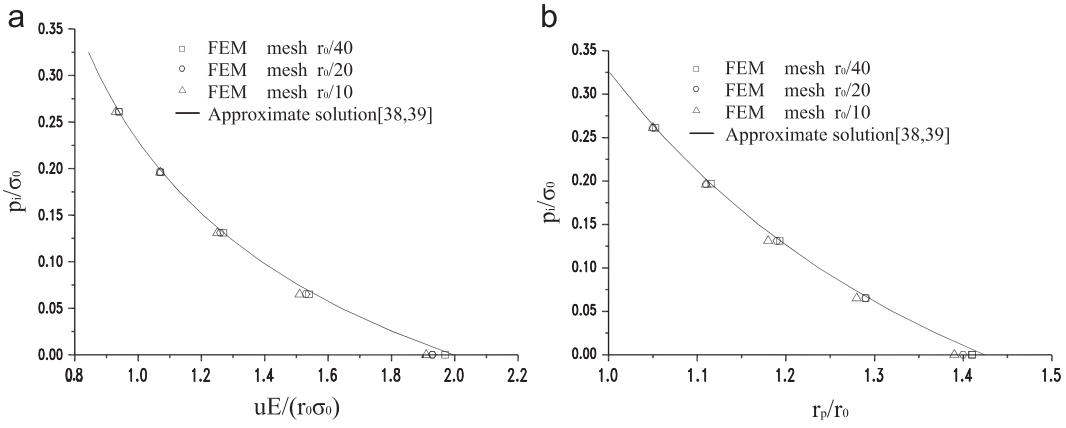

Fig. 9. Approximate solution and results by FEM with different mesh sizes, (a) ground reaction curve and (b) evolution of plastic radii for rock mass #1.

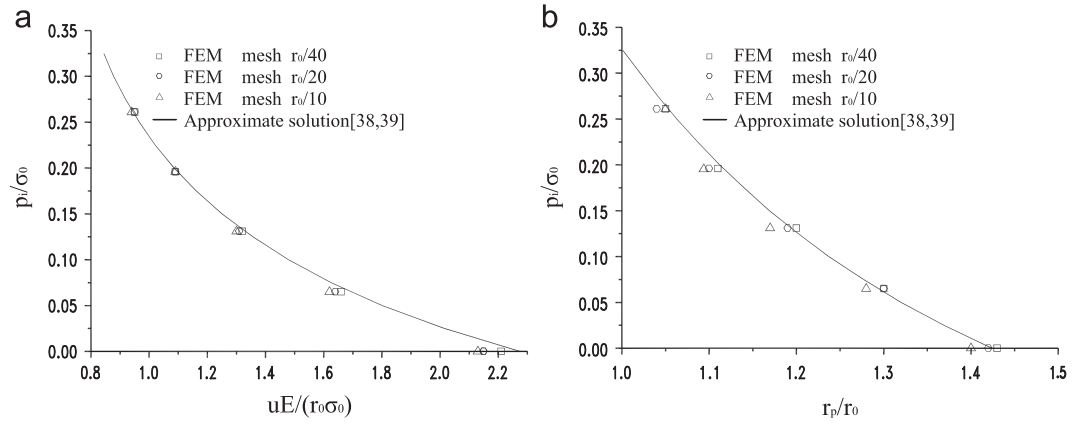

Fig. 10. Approximate solution and results by FEM with different mesh sizes, (a) ground reaction curve and (b) evolution of plastic radii for rock mass #2.

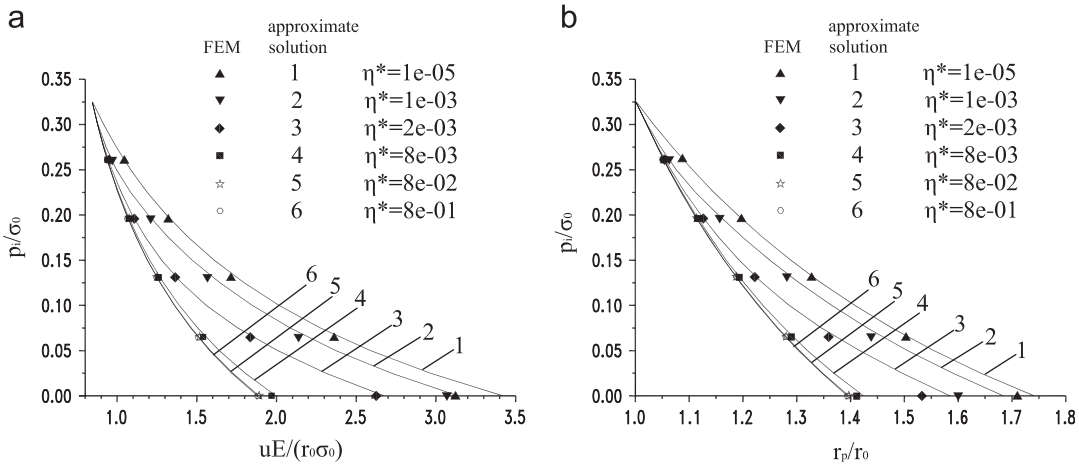

Fig. 11. Approximate solution and results by FEM with different softening parameters, (a) ground reaction curve and (b) evolution of plastic radii for rock mass #1.

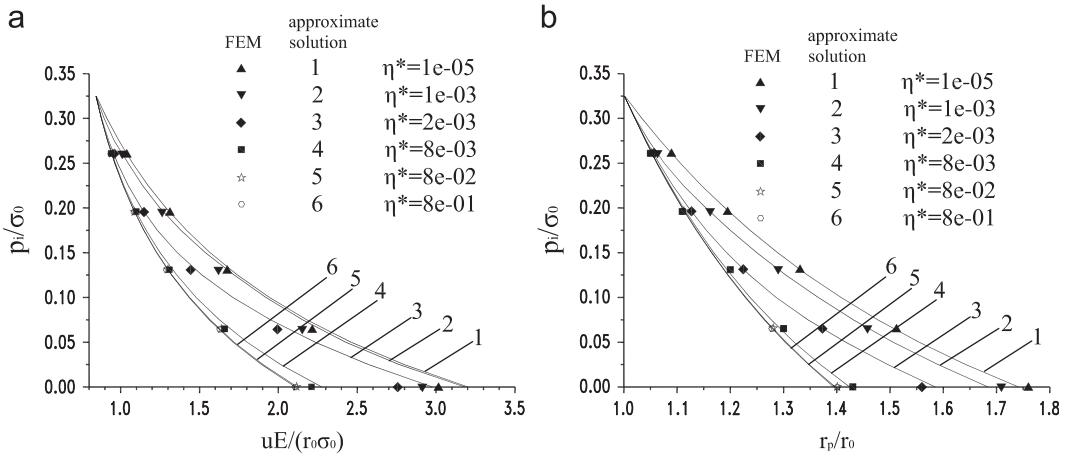

Fig. 12. Approximate solution and results by FEM with different softening parameters, (a) ground reaction curve and (b) evolution of plastic radii for rock mass #2.

This numerical example is used to validate the finite element implementation of the proposed method and check the effectiveness of handling any softening slopes by employing different softening parameters (η^*). Therefore, the following analyses are carried out below:

(i) Parameters of M–C rock mass with #1 and #2 are used, and dimensionless forms of the displacement ($uE/\sigma_0 r_0$) and the radius of the plastic region (r_p/r_0) are displayed when the internal pressure (p_i) change from $p_i=p_c$ to $p_i=0$. Meanwhile, different softening parameters (η^*) are analyzed and the corresponding numerical results are presented.

(ii) Numerical results are compared with those obtained by the methods [38–39].

The numerical results are displayed in ground response curves and evolution of plastic radii. All of the results by FEM and those

by approximate methods corresponding to different softening parameters (η^*) are shown in Fig. 11 for rock mass #1 and Fig. 12 for rock mass #2. The comparison of the results by the proposed method with those by approximate approach [38,39] is made.

When the magnitude of the critical plastic shear strain (η^*) changes from big to small, for example, from $\eta^*=8e-1$ to $\eta^*=1e-5$, it means that the softening slope changes from gentle to steep and that the geo-material behaves from elastic-perfectly plasticity to elastic-brittle-plasticity. Accordingly, the plastic zone and the deformation increase in the surrounding rock mass as the critical plastic shear strain (η^*) decreases. This phenomenon is observed in both Figs. 11 and 12. In fact, when $\eta^*=1e-05$, the softening slope is so steep that the problem becomes the brittle-plastic one, and when $\eta^*=8e-01$, the softening slope is so gentle that it can be regarded as an elasto-perfectly plastic one. The results in Figs. 11 and 12 show that strain-softening solution converges to the brittle-plastic solution when η^* decreases and it converges to the elasto-perfectly plastic one when η^* increases.

From Figs. 11 and 12, the numerical results demonstrate that the solutions by FEM is generally in agreements with those by approximate methods whether the softening parameter (η^*) is big or small. This indicates that the proposed method can deal with different softening slope whether it is steep or gentle. Figs. 11 and 12 also shows that the relative error between the results by the proposed finite element implementation and those by approximate solutions will increase as η^* becomes small (i.e. the softening slope becomes steep). The differences may be caused by the assumption made in FEM and in the approximate methods.

In the method of [38,39], the axisymmetric condition is enforced, and no bifurcation or localization phenomena will appear in the axisymmetric solutions, whereas no axisymmetric conditions are assumed when the presented numerical method is used to study the deformation and plastic zone in strain-softening material.

The localization phenomena appear in the plastic zone as the steep softening slope is modeled. Fig. 13(a) and (b) shows the plastic regions around the tunnel surface for the softening parameter $\eta^*=1e-05$ and $\eta^*=8e-01$ for rock mass #1, respectively. In Fig. 13(a), the interface between the elastic and the plastic zone is not smooth because of the localization phenomena. The radius of the plastic annulus presented in Fig. 11 (and Fig. 12) is determined by the area of plastic region in this case. It means that the equivalent area of the plastic annulus is equal to that of the computed plastic region. Numerical analysis shows that the area of the plastic region is generally the same with different mesh sizes although the shape of the region may be mesh dependent for strain-softening rock mass. In regard to the displacement presented in Figs. 11 and 12, it should be noted that the radial displacement is the average of the radial displacements of all the nodes around the tunnel face.

For the clearness of the magnitude of equivalent plastic radius and displacement at the tunnel wall shown in Figs. 11 and 12, Tables 2 and 3 present their numerical values when the internal pressure $p_i=0$.

5.2. Example 2. Engineering application—a large cavern excavated in hard rock masses

Fig. 14(a) and (b) shows a geological cross-section at the middle of the generator room in an underground power station. The rock mass is slightly weathered and fresh granite gneiss. A thick seam mainly consisting of mylonite runs parallel to the longitudinal axis of the generator room which has the maximum width of 27 m and height of 71 m. The generator room is excavated in 5 steps. Plane strain condition is assumed. The finite element mesh is shown in Fig. 14(c) and (d).

The initial stress in rock mass is computed through the self-weight in the vertical direction and $\sigma_x=1.53\gamma h$, where γ is the

Table 2
Numerical results for rock mass #1 when the internal pressure $p_i=0$ (Data in parenthesis are solutions by the methods of Lee and Pietruszczak [38] and Wang et al. [39]).

η^*	r_p/r_0	$uE/\sigma_0 r_0$
$1e-05$	1.71 (1.74)	3.17 (3.42)
$1e-03$	1.60 (1.68)	3.09 (3.14)
$2e-03$	1.53 (1.58)	2.65 (2.67)
$8e-03$	1.41 (1.42)	1.97 (1.99)
$8e-02$	1.39 (1.40)	1.88 (1.89)
$8e-01$	1.39 (1.39)	1.88 (1.89)

Table 3
Numerical results for rock mass #2 when the internal pressure $p_i=0$ (Data in parenthesis are solutions by the methods of Lee and Pietruszczak [38] and Wang et al. [39]).

η^*	r_p/r_0	$uE/\sigma_0 r_0$
$1e-05$	1.76 (1.74)	3.02 (3.20)
$1e-03$	1.71 (1.68)	2.91 (3.19)
$2e-03$	1.56 (1.58)	2.76 (2.98)
$8e-03$	1.43 (1.42)	2.21 (2.27)
$8e-02$	1.40 (1.40)	2.12 (2.12)
$8e-01$	1.40 (1.39)	2.12 (2.12)

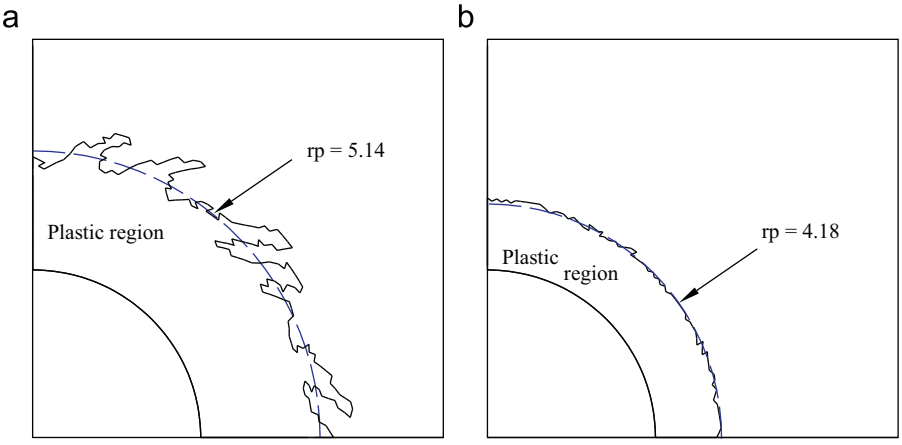

Fig. 13. Plastic regions and the equivalent plastic radius around the tunnel for (a) $\eta^*=1e-05$, (b) $\eta^*=8e-01$ for rock masses #1.

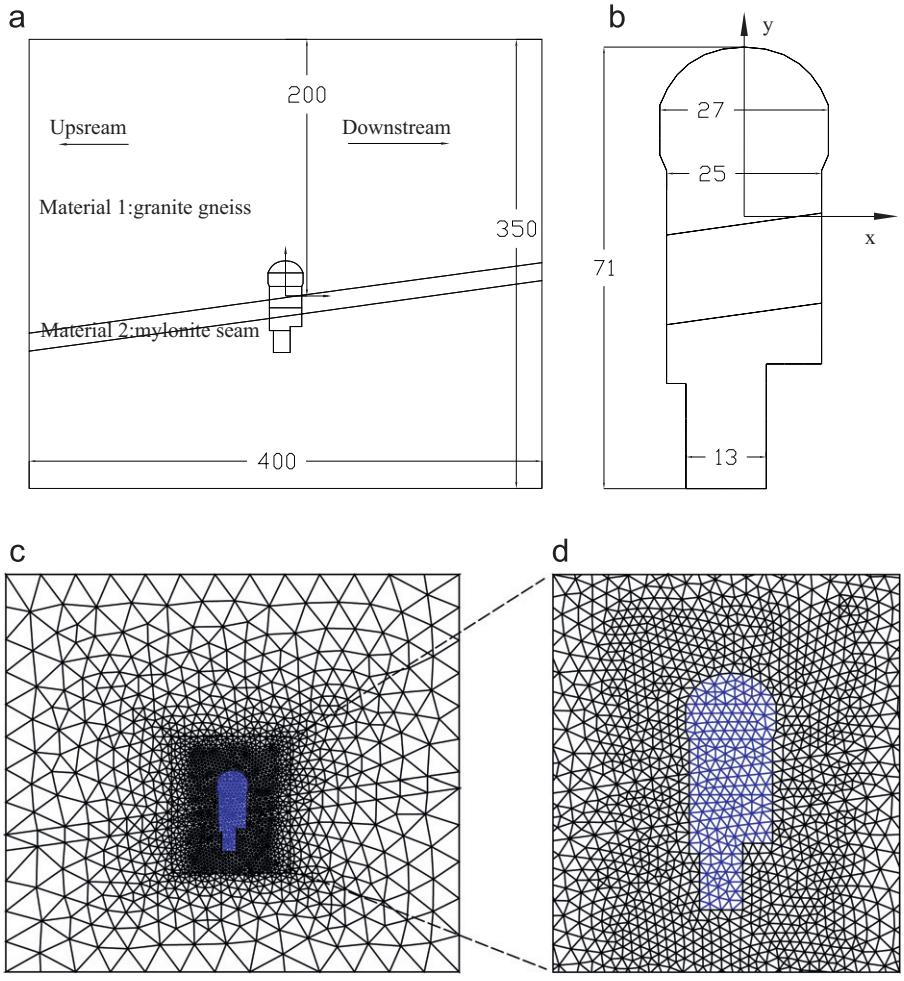

Fig. 14. (a) geometry of the geological cross-section, (b) the generator room,(c) finite element mesh with 3745 elements and 1899 nodes, (d) finite element mesh around the generator room.

Table 4
Mechanical parameters.

M–C rock mass	Material 1	Material 2
Young's modulus, E (GPa)	20	3.5
Poisson's ratio (v)	0.25	0.25
Density (KN/m^3)	27	26.7
η^*	0.002	0.004
c_p (MPa)	1.2	0.3
c_r (MPa)	0.8	0.1
φ_p (deg.)	47.3	35.5
φ_r (deg.)	40.3	20.5
ψ_p (deg.)	47.3	35.5
ψ_r (deg.)	40.3	20.5
σ_{tp} (MPa)	1.0	0.3
σ_{tr} (MPa)	0.5	0.1

unit weight and h is the depth from the ground surface. Two kinds of rock masses are included in the model and their mechanical parameters are presented in Table 4.

Elasto-perfectly plastic, elasto-plastic strain-softening and elastic-brittle-plastic analyses are carried out for the problem, and the plastic zones are shown in Fig. 15 after the completion of excavation. The plastic zones are formed in the surrounding rock masses. It is indicated in fence lines for elasto-perfectly plastic model, in track symbols for elasto-plastic strain-softening model and in zigzag lines for elasto-perfectly brittle-plastic analysis. The maximum depth of the plastic zone for the analyses is 16.2, 19.1 and 27.2 m, respectively.

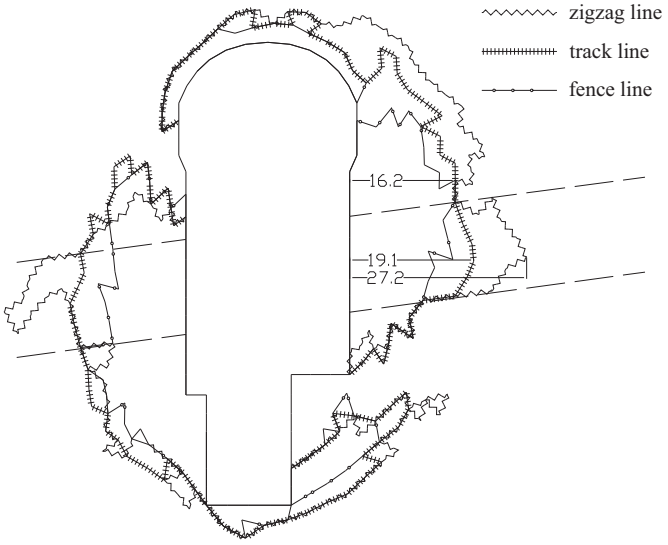

Fig. 15. Plastic zones of elasto-perfectly plastic, elasto-plastic strain-softening and elasto-perfectly brittle-plastic models(fence line for elasto-perfectly plastic model, track line for strain-softening model and zigzag line for brittle-plastic model).

It is obvious that the plastic area for elasto-perfectly plastic model is the smallest among the analyses, so is the maximum depth of the plastic zone. The magnitude of the plastic area and the maximum depth of plastic zone is in the middle for elasto-plastic strain-softening model, and it is the biggest for elastic-brittle-plastic analysis.

Considering that the peak and residual strengths of the rock are observed in laboratory test, we think that the elasto-plastic strain-softening and elastic-brittle-plastic analyses are appropriate. Probably the design of support is a little conservative if the results of the elastic-brittle-plastic analysis are used. But it is risky that the results of the elasto-perfectly plastic model are utilized for the design of support because there are about 3 m difference in the maximum depth of the plastic zone between strain-softening and elasto-perfectly plastic analyses. In practice, anchorage cables had to be added in the upper and middle part of the generator room and numerical analysis provides the basic data for the support design. With the consideration of the strain-softening behavior common in geo-material, elasto-plastic strain-softening analysis should be paid attention to when the plastic region and deformation are concerned in the excavation of tunnels and in geotechnical engineering such as cut-slopes.

6. Conclusions

This paper proposed a new finite element implementation for strain-softening constitutive model. In the proposed implementation, strain-softening process is simplified as a series of stress drop and plastic flow, and solving a strain-softening problem becomes finding a series of brittle-plastic solutions. Thereby, the limitation to the rate of softening, as well as numerical instability, is overcome when strain-softening problem is analyzed by means of numerical methods within the framework of the classical theory of plasticity.

The presented analytical and numerical procedure for strain-softening material is validated by a simple example in which plastic zone and deformation of rock mass are obtained with different rate of softening. Comparison of results indicates that the macroscopic response of the tunnel excavation in plastic region and displacements does not differ significantly from that expected by approximate approaches [38,39] even if localization phenomena occurs in the plastic zone.

The engineering application case shows that differences in both plastic area and the depth of plastic zone are pronounced between elasto-perfectly plastic and strain-softening (and brittle-plastic) analyses. The differences will influence the design of support and the stability of the underground caverns. Therefore, it is important to consider the strain-softening behavior in geotechnical engineering.

Acknowledgements

The authors thank the State Key Laboratory of Geomechanics and Geotechnical Engineering for financial support of the research project entitled 'Research on the Mechanical Properties and Analysis Method of Continuous and Discontinuous Rock Mass' under contract reference numbers (SKLQ005 and SKLZ0802). Thanks are also given to the editor and the two anonymous reviewers for their valuable comments which will make the paper much better than the initial manuscript.

References

[1] Zheng H, Liu DF, Lee CF, Ge XR. Principle of analysis of brittle-plastic rock mass. Int J Solids Struct 2005;42:139–58.
[2] Hoek E, Brown ET. Practical estimates of rock mass strength. Int J Rock Mech Min Sci Geomech 1997;34:1165–87.
[3] Read HE, Hegemier GA. Strain softening of rock, soil and concrete-a review article. Mech Mater 1984;3:271–94.
[4] Cundall PA. Numerical experiments on localization in frictional materials. Arch Appl Mech 1989;59:148–59.
[5] Bardet JP, Proubet J. A numerical investigation of the structure of persistent shear bands in granular media. Geotechnique 1991;41:599–613.
[6] Asaro RJ, Rice JR. Strain localization in ductile single crystals. J Mech Physics Solids 1977;25:309–38.
[7] Wong TF. Micromechanics of faulting in Westerly granite. Int J Rock Mech Min Sci 1982;19:49–62.
[8] Fredrich JT, Wong TF. Micromechanics of thermally induced cracking in three crustal rocks. J Geophys Res 1986;91:12743–64.
[9] Fredrich JT, Evans B, Wong TF. Micromechanics of the brittle to plastic transition in Carrara marble. J Geophys Res 1989;94:4129–45.
[10] Kemeny JM, Cook NGW. Micromechanics of deformation in rocks. In: Shah SP, editor. Toughening Mechanics in Quasi-Brittle Materials. Dordrecht: Kluwer; 1991. p. 155–88.
[11] de Borst R. Simulation of strain localization: a reappraisal of the Cosserat continuum. Eng Comput 1991;8:317–32.
[12] Muhlhaus HB, Vardoulakis I. The thickness of shear bands in granular materials. Geotechnique 1987;37:271–83.
[13] Bazant ZP, Belytschko T, Chang TP. Continuum theory for strain-softening. J Eng Mech ASCE 1984;110:1666–92.
[14] Pijaudier-Cabot G, Bazant ZP. Nonlocal damage theory. J Eng Mech ASCE 1987;113:1512–33.
[15] de Borst R, Muhlhaus HB. Gradient-dependent plasticity: formulation and algorithm aspects. Int J Num Meth Eng 1992;35:521–39.
[16] de Borst R, Muhlhaus HB, Pamin J. Fundamental issues in finite element analysis of localization of deformation. Eng Comput 1993;10:99–121.
[17] Roy AB, Marc GD, Frank PT. Nonlocal implicit gradient-enhanced elasto-plasticity for the modelling of softening behaviour. Int J Plast 2003;19:403–33.
[18] Regueiro RA, Borja RI. A finite model of localized deformation in frictional material taking a strong discontinuity approach. Finite Elem Anal Des 2000;33:283–315.
[19] Wells GN, Sluys LJ. Three-dimensional embedded discontinuity model for brittle fracture. Int J Solids Struct 2001;38:897–913.
[20] Belytschko T. A finite element with embedded localization zones. Comput Meth Appl Mech Eng 1988;70:59–89.
[21] Samaniego E, Belytschko T. Continuum-discontinuum modelling of shear bands. Int J Num Meth Eng 2005;62:1857–72.
[22] Pietruszczak S, Mroz Z. Finite element analysis of deformation of strain-softening materials. Int J Num Meth Eng 1981;17:327–34.
[23] Larsson R, Runesson K, Sture S. Finite element simulation of localized plastic deformation. Arch Appl Mech 1991;61:305–17.
[24] Pietruszczak S, Niu X. On the description of localized deformation. Int J Numer Anal Meth Geomech 1993;17:791–805.
[25] Bardet JP. A comprehensive review of strain localization in elastoplastic soils. Comp Geotech 1990;10:163–88.
[26] Pietruszczak S, Xu G. Brittle response of concrete as a localization problem. Int J Solids Struct 1995;32:1517–33.
[27] Sterpi D. An analysis of geotechnical problems involving strain softening effects. Int J Numer Anal Meth Geomech 1999;23:1427–54.
[28] Lo KY, Lee CF. Stress analysis and slope stability in strain-softening material. Geotechnique 1973;23:1–11.
[29] Zhang W, Subhash G. An elastic–plastic-cracking model for finite element analysis of indentation cracking in brittle materials. Int J Solids Struct 2001;38:5893–913.
[30] Hajiabdolmajida V, Kaisera PK, Martin CD. Modeling brittle failure of rock. Int J Rock Mech Min Sci 2002;39:731–41.
[31] Krajcinovic D, Vujosevic M. Intrinsic failure modes of brittle materials. Int J Solids Struct 1998;35:2487–503.
[32] Ju JW. On the energy based coupled elastoplastic damage theories: constitutive modeling and computational aspects. Int J Solids Struct 1989;25:803–33.
[33] Etienne FH, Hoxha D, Shao JF. A continuum damage constitutive law for brittle rocks. Comp Geotech 1998;22:135–51.
[34] Chiarelli AS, Shao JF, Hoteit N. Modeling of elastoplastic damage behavior of a claystone. Int J Plast 2003;19:23–45.
[35] Giang DN, Guy TH. A coupled damage–plasticity model for concrete based on thermodynamic principles: Part II: non-local regularization and numerical implementation. Int J Numer Anal Meth Geomech 2008;32:391–413.
[36] Varas F, Alonso E, Alejano LR, Fdez-Manin G. Study of bifurcation in the problem of unloading a circular excavation in a strain-softening material. Tunnel Underground Space Technol 2005;20:311–22.
[37] Zienkiewicz OC, Taylor RL. The finite element method. New York: McGraw-Hill; 1991.
[38] Lee YK, Pietruszczak S. A new numerical procedure for elasto-plastic analysis of a circular opening excavated in a strain-softening rock mass. Tunnel Underground Space Technol 2008;23:588–99.
[39] Wang SL, Yin XT, Tang H, Ge XR. A new approach for analyzing circular tunnel in strain-softening rock masses. Int J Rock Mech Min Sci 2010;47:170–8.
[40] Alonso E, Alejano LR, Varas F, Fdez-Manin G, Carranza-Torres C. Ground response curves for rock masses exhibiting strain-softening behavior. Int J Numer Anal Meth Geomech 2003;27:1153–85.